

Featureless Visual Navigation using Optical Flow of Omnidirectional Image Sequence

Yoshihiko Mochizuki¹ and Atsushi Imiya²

¹ Graduate School of Advanced Integration Science, Chiba University, Japan

² Institute of Media and Information Technology, Chiba University, Japan
Yayoi-cho 1-33, Inage-ku, Chiba 263-8522, Japan

Abstract. In this paper, we develop a featureless visual navigation algorithm for the autonomous robot mounting a spherical imaging system. The spherical image is the normalised image for omnidirectional images. Differences of the depth from the camera to the objects yield the disparity on the image. Using the disparity of optical flow vectors on the spherical image, we construct a method to compute the direction for navigation. For the computation of the optical flow vectors, we develop the Horn-Schunck method on the spherical images.

1 Introduction

In this paper, we develop a visual navigation method for the autonomous robot using optical flow on the spherical image. The spherical image is the normalised image for omnidirectional images. The spherical image expression of the omnidirectional images provides the imaging-system-free expression of omnidirectional images. The view from a compound eye of insects and birds yield a spherical image. Animals which observe spherical images decide the navigation direction from a sequence of spherical images. Especially, the compound-eye of insects detects moving objects in the environment and egomotion from optical flow. Therefore, we construct an algorithm to compute the free space and the navigation direction from the sequence of optical flow fields of the spherical images. The use of optical flow fields allows the robot to navigate without any features and landmarks in the workspace [17–19].

In a real environment, the payload of a mobile robot, for example, power supply, capacity of input devices and computing power, is restricted. Therefore, mobile robots are required to have simple mechanisms and devices [11, 17]. The vision sensors provide low-cost devices that is easily mounted on mobile robots. As same as the pinhole camera system, geometrical features such as lines and planes in the environment are fundamental cues to the configuration of obstacles in the three-dimensional space. If we adopt these traditional strategies, the robot is required to detect the free space as the dual of the space occupied by obstacles. Furthermore, if the map of workspace is used for the navigation, the robot is required to prepare geometrical transformation method to transform the omnidirectional view to the map. These two methodologies require special

memories to the robot for the visual navigation. However, the method which uses optical flow computed from images captured by a robot-mounted imaging system is suitable for the small payload robot, since the optical-flow-based method provides a featureless algorithm for the visual navigation [17–19].

Omnidirectional vision system allows the robot to observe the back view in which the robot has safely navigated without colliding to the obstacles, that is, the back view in the omnidirectional image captures the region which was a free space in the past on the path of the robot. This property of the omnidirectional view captured by the camera mounted on the robot allows the robot to use back views as features for the free space detection in the front view. Therefore, using back view of the omnidirectional images, it is possible to reduce the memory capacity for the visual navigation. Furthermore, using the norm of the optical flow vectors on the sphere, we define the potential to control the navigation direction. Our method proposed in this paper uses the back view captured by an omnidirectional vision system [5, 20] as a temporal model for the featureless visual navigation.

2 Related Works

The omnidirectional vision system is widely used in surveillance and robot navigation [14, 8, 22]. Using the wide view of the omnidirectional imaging system, in the surveillance and the robot navigation, the moving objects in the wide area and the landmarks in the wide area are detected for inspection and robot localisation, respectively. For the robot navigation, omnidirectional or panoramic views allow us to compute simply the position of the robot using the several landmarks in the omnidirections detected simultaneously by a single camera. This geometrical advantage is the most important property of the omnidirectional imaging system mounted on the autonomous robot.

For the robot navigation in an environment without any landmarks, such as a new environment without any configuration maps for the robot, the detection of the free space and free directions, in which robot can move without any collision to the obstacles, is a fundamental task. Ohnishi and Imiya [17], Sobey [18], Santos-Victor [19] and Braillon *et al* [3] developed an algorithm for the free space detection using the sequence optical flow fields computed from images captured by a pinhole camera system mounted on the mobile robot, since the autonomous robot with the vision system automatically detects a sequence of images using the vision system mounted on the robot.

Navigation using the focus of expansion (FOE) and the focus of conversion (FOC) [13, 15] is a simple method to decide the direction of the egomotion of the robot, since the vector from the FOC to the FOE coincides the direction of the egomotion [7, 15]. Therefore, the detection of these two focus points is an essential task for the visual navigation using optical flow on the spherical images.

Using a vision system inspired by insects, navigation algorithms for the autonomous robot are proposed [6, 7, 10, 18, 21]. The insect-inspired vision for robot control [21, 23] uses simple information observed by the vision system mounted

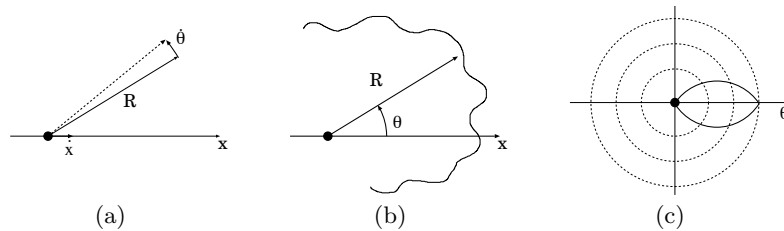


Fig. 1. Insect-inspired range navigation. (a)-(c) Insect inspired range potential. An insect understands the range data in the eye-centred coordinates using the optical flow field observed while it is flying around the environment. This range data observed by the moving camera (eye) yields the range-based potential field around the insect for navigation to the local destination. (a) Motion and optical flow. (b) Range data in the eye-centred coordinate. (c) The range-based potential for control to the local destination. In these figures, \dot{x} , $\dot{\theta}$, and R are the velocity of the insect, the angular velocity of objects, and the distance to the object, respectively. Then, the relationship $\dot{\theta} = \dot{x} \sin \frac{\theta}{R}$ are satisfied.

on the robot. Optical flow is a feature computed from a sequence of temporal images. A sequence of temporal images are automatically captured by a moving camera, such as an imaging system mounted on the autonomous mobile robot. This navigation method uses the vector from the FOC to the FOD as the visual compass.

Autonomous vehicles use optical flow field as a fundamental cue for the navigation. Sobey [18] introduced a control strategy for robot navigation using optical flow and the potential field. Considering a camera moving along its optical axis with a velocity \dot{x} , the angular velocity of objects across the image plane of a moving camera can be expressed as $\dot{\theta} = \dot{x} \sin \frac{\theta}{R}$, where θ is the angular position of an object on the image plane with respect to the direction of motion, $\dot{\theta}$ is the angular velocity of the object image, and R is the distance to the object. Sobey used the relationship between optical flow and range, which is possibly used by insects for the detection of obstacles in the space for motion control, as shown in Figs. 1(a)-(c). This range in the space detected by the optical flow observed by the camera is used for the generation of the potential, which is used for the computation of the control force to avoid collision with obstacles. Furthermore, Sobey used low-resolution images to overcome the inaccuracy of range detection from optical flow. The view from the eyes of flying birds and the compound eyes of the insects is a spherical image, which is a standard image for images captured by the omnidirectional vision system.

To achieve programs in refs. [18] and [23] using an omnidirectional vision system, we are required to compute optical flow from the sequence omnidirectional images [5, 20]. Therefore, in this paper, we propose an accurate method to compute optical flow for the spherical images captured by a catadioptric omni-

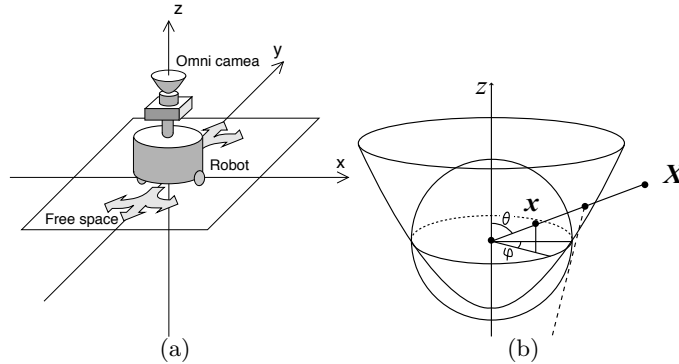


Fig. 2. Geometry of the catadioptric camera system and optical flow on the spherical camera. (a) The robot mounting a catadioptric omnidirectional system moves on the ground floor. The optical axis of the camera system is perpendicular to the ground floor. The robot moves as the combination of the rotation around the gravity axis of the robot and the translation. (b) Setting that the camera centre to be at the centre of the coordinate system, the spherical camera transforms the point $\mathbf{X} = (X, Y, Z)^T \in \mathbf{R}^3$ to the point $\mathbf{x} = \frac{\mathbf{X}}{|\mathbf{X}|}$ on the sphere.

directional imaging system. as the normalised images. In this paper, using depth information from optical-flow of translation motion on the spherical image, we develop an algorithm to compute the navigation direction. In ref. [17], three successive images are used for the featureless visual navigation. In the algorithm a temporal model is generated from the first pair of images from three images.

3 Optical Flow Computation on the Sphere

In this paper, we assume that the spherical images are generated from images captured by the catadioptric camera systems. Setting that the camera centre to be at the centre of the coordinate system, the spherical camera transforms the point $\mathbf{X} = (X, Y, Z)^T \in \mathbf{R}^3$ to the point $\mathbf{x} = \frac{\mathbf{X}}{|\mathbf{X}|}$ on the sphere.

Figure 2 shows geometry of the catadioptric camera system mounted on the mobile robot. The robot moves on the ground floor. The optical axis of the camera system is perpendicular to the ground floor. The robot moves as the combination of the rotation around the gravity axis of the robot and the translation. Setting that the camera centre to be at the centre of the coordinate system, the spherical camera transforms the point $\mathbf{X} = (X, Y, Z)^T \in \mathbf{R}^3$ to the point $\mathbf{x} = \frac{\mathbf{X}}{|\mathbf{X}|}$ on the sphere. On the spherical camera, we use the spherical coordinate $(\sin \theta \cos \phi, \sin \theta \sin \phi, \cos \theta)^T$.

Setting $\mathbf{x} = (x, y, z)^T$ to be a point on a space \mathbf{R}^3 , for $0 \leq \theta \leq \pi$ and $0 \leq \phi < 2\pi$, a point on the unit sphere is parameterised as $x = \cos \phi \sin \theta$, $y = \sin \phi \sin \theta$, and $z = \cos \theta$. Therefore, a function on the unit sphere S^2 is

parameterised as $I(\theta, \phi)$. The vector expression of the spatial gradient on the unit sphere is $\nabla_S = \left(\frac{\partial}{\partial \theta}, \frac{1}{\sin \theta} \frac{\partial}{\partial \phi} \right)^\top$.

For temporal image $f(\theta, \phi, t)$ on the unit sphere S^2 , the total derivative [5] is

$$\frac{d}{dt}f = \frac{\partial}{\partial \theta}f + \frac{1}{\sin \theta} \frac{\partial}{\partial \phi}f + \frac{\partial}{\partial t}f. \quad (1)$$

The solution $\mathbf{u} = (\dot{\theta}, \dot{\phi})^\top = (p(\theta, \phi), q(\theta, \phi))^\top = (p, q)^\top$ of the equation

$$\nabla_S f^\top \mathbf{u} + \partial_t f = 0, \quad (2)$$

for $\partial_t f = \frac{\partial f}{\partial t}$, is optical flow of image I on the unit surface S^2 . The computation of optical flow from eq. (2) is an ill-posed problem. The Horn-Schunck criterion for the computation of optical flow [12] on the unit sphere is expressed as the minimisation of the functional

$$J(p, q) = \int_{S^2} \{ |\nabla_S f^\top \mathbf{u} + \partial_t f|^2 + \alpha (\|\nabla_S p\|_2^2 + \|\nabla_S q\|_2^2) \} \sin \theta d\theta d\phi, \quad (3)$$

where L_2 norm on the unit sphere is defined by

$$\|f(\theta, \phi)\|_2^2 = \int_{S^2} |f(\theta, \phi)|^2 \sin \theta d\theta d\phi. \quad (4)$$

The Euler-Lagrange equation of this minimisation problem is

$$\nabla_S^\top \nabla_S \mathbf{u} = \frac{1}{\alpha} (\nabla_S f^\top \mathbf{u} + \partial_t f) \nabla_S f \quad (5)$$

and the associated diffusion equation is

$$\frac{\partial}{\partial t} \mathbf{u} = \nabla_S^\top \nabla_S \mathbf{u} - \frac{1}{\alpha} (\nabla_S f^\top \mathbf{u} + \partial_t f) \nabla_S f. \quad (6)$$

For numerical computation of the equation, we use semi-explicit discretization

$$\frac{\mathbf{u}_{mn}^{l+1} - \mathbf{u}_{mn}^l}{\Delta \tau} = \nabla_S^\top \nabla_S \mathbf{u}_{mn}^n - \frac{1}{\alpha} ((\nabla_S f)_{mn}^\top \mathbf{u}_{mn}^{l+1} + (\partial_t f)_{mn}) (\nabla_S f)_{mn} \quad (7)$$

for sampled optical flow field $\mathbf{u}_{ij} = (p_{ij}, q_{ij})^\top$, $p_{mn} = p(hm, hn)$ such that $0 < p_{ij} < \pi$, and $q_{mn} = v(hm, hn)$, where h is the unit sample interval, and $\Delta \tau$ is a small positive value.

Equation (7) derives the iteration equation

$$\left(\mathbf{I} + \frac{\Delta \tau}{\alpha} \mathbf{S}_{mn} \right) \mathbf{u}_{mn}^{(l+1)} = \mathbf{u}_{mn}^{(l)} + \mathbf{l}_S \mathbf{u}_{m-i, n-j}^{(l)} + \frac{1}{\kappa} \mathbf{c}_{mn}, \quad l \geq 0, \quad (8)$$

where

$$\mathbf{S}_{mn} = (\nabla_S f)_{mn} (\nabla_S f)_{mn}^\top, \quad \mathbf{c}_{mn} = (\partial_t f)_{mn} (\nabla_S f)_{mn}. \quad (9)$$

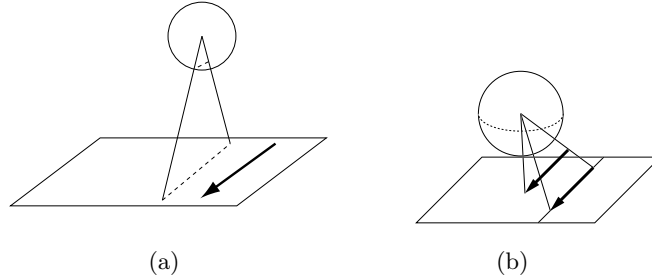


Fig. 3. Disparity of Optical Flow Vectors (a) The translation of the robot causes the translation optical-flow. The translation optical flow vectors are the tangent vectors to the bundle of great circles which are the projection of the bundle of parallel lines in the space. (b) The difference of depths of infinitesimal coplanar parallel vectors affects to the length of optical-flow vectors.

for

$$(\nabla_S f)_{ij} = \frac{1}{2} \begin{pmatrix} 1 & 0 \\ 0 & \sin \theta_i \end{pmatrix} \begin{pmatrix} f_{i+1j} - f_{i-1j} \\ f_{ij+1} - f_{ij-1} \end{pmatrix} \quad (10)$$

and the discrete operation $\mathbf{l}_S = \nabla_s^\top \nabla_s$ on the sphere

$$\mathbf{l}_S \mathbf{u}_{ij} = \begin{pmatrix} \frac{1}{2}(p_{i+1j} + p_{i-1j}) + \frac{1}{2\sin^2 \theta_i}(p_{ij+1} + p_{ij-1}) - (1 + \frac{1}{\sin^2 \theta_i})p_{ij} \\ \frac{1}{2}(q_{i+1j} + q_{i-1j}) + \frac{1}{2\sin^2 \theta_i}(q_{ij+1} + q_{ij-1}) - (1 + \frac{1}{\sin^2 \theta_i})q_{ij} \end{pmatrix}. \quad (11)$$

4 Disparity of Optical Flow

In this paper, we assume that a robot with a system of catadioptric omnidirectional imaging system moves on a flat ground floor with some obstacles. The optical flow vectors on the unit sphere are projections of the infinitesimal vectors on a collection of parallel lines to the sphere as shown in Fig. 4(a). Using this geometrical property of the optical flow vectors, we derive geometric structure of the optical flow on the sphere. For the computation of the geometrical structure of the optical flow, we adopt the cylindrical coordinate system to express the location of the point in the space as $\mathbf{X} = (R \cos \phi, R \sin \phi, Z)^\top$. The point \mathbf{P} in the space is transformed to the point

$$\mathbf{x} = \left(\frac{R}{\sqrt{R^2 + Z^2}} \cos \phi, \frac{R}{\sqrt{R^2 + Z^2}} \sin \phi, \frac{Z}{\sqrt{R^2 + Z^2}} \right)^\top \quad (12)$$

on the spherical image. We assume that the motion of the robot is piecewise line.

Points on the line $\mathbf{X} = D\mathbf{e}_1 + t\mathbf{e}_2 + Z\mathbf{e}_3$, $-\infty \leq t \leq \infty$, where $\mathbf{e}_1 = (1, 0, 0)^\top$, $\mathbf{e}_2 = (0, 1, 0)^\top$ and $\mathbf{e}_3 = (0, 0, 1)^\top$, are expressed as

$$\mathbf{P} = (D|\tan \phi| \cos \phi, D|\tan \phi| \sin \phi, Z)^\top, \quad (13)$$

using the cylinder coordinate. The image of the point \mathbf{P} is

$$\mathbf{p} = \frac{1}{\sqrt{D^2 \tan^2 \phi + Z^2}} \mathbf{P}. \quad (14)$$

Setting the points \mathbf{P} and $\mathbf{P}' = \mathbf{P} + \Delta$, where Δ is an infinitesimal vector, to be a pair of points in the space, the optical-flow vector on the spherical camera is

$$\frac{\Delta \mathbf{p}}{\Delta t} = \frac{\mathbf{P}'}{|\mathbf{P}'|} - \frac{\mathbf{P}}{|\mathbf{P}|} = \mathbf{p}' - \mathbf{p}, \quad (15)$$

where \mathbf{p} and \mathbf{p}' are the images of \mathbf{P} and \mathbf{P}' , respectively. Therefore, on the unit sphere, the optical flow vector of the translation is expressed in the cylinder coordinate as

$$\mathbf{v}(r, \phi, z) = \sqrt{\frac{D \tan^2 \phi}{D^2 \tan^2 \phi + Z^2}} \begin{pmatrix} \mathbf{m} \\ Z \cot \phi \end{pmatrix}, \quad \mathbf{m} = \begin{cases} \mathbf{n}^\perp, & \text{if } |\phi| \leq \frac{1}{2}\pi, \\ -\mathbf{n}^\perp, & \text{otherwise.} \end{cases} \quad (16)$$

where $\mathbf{n} = (\cos \phi, \sin \phi)^\top$ and $\mathbf{n}^\perp = (-\sin \phi, \cos \phi)^\top$.

Vectors

$$\mathbf{P} = (D |\tan \phi| \cos \phi, D |\tan \phi| \sin \phi, Z)^\top, \quad \mathbf{P}' = \mathbf{P} + \Delta \quad (17)$$

and

$$\mathbf{Q} = \left(\frac{Z-s}{Z} D |\tan \phi| \cos \phi, \frac{Z-s}{Z} D |\tan \phi| \sin \phi, (Z-s) \right)^\top, \quad \mathbf{Q}' = \mathbf{Q} + \Delta, \quad (18)$$

for $|D| > s > 0$ and $\Delta = \Delta \mathbf{e}_2$ where $\mathbf{e}_2 = (0, 1, 0)^\top$, satisfy the relation $|\mathbf{Q}' - \mathbf{Q}| = |\mathbf{P}' - \mathbf{P}|$ and vectors $(\mathbf{Q}' - \mathbf{Q})$ and $(\mathbf{P}' - \mathbf{P})$ are coplanar. Therefore, setting \mathbf{p}' , \mathbf{p} , \mathbf{q}' , and \mathbf{q} to be the images of \mathbf{P}' , \mathbf{P} , \mathbf{Q} , and \mathbf{Q}' on the unit sphere, respectively, we have the relation

$$\left| \frac{\mathbf{p}' - \mathbf{p}}{\Delta t} \right| = \left| \frac{\Delta \mathbf{p}}{\Delta t} \right| < \left| \frac{\Delta \mathbf{q}}{\Delta t} \right| = \left| \frac{\mathbf{q}' - \mathbf{q}}{\Delta t} \right|. \quad (19)$$

Equation (19) shows that the depth affects to the length of optical-flow vectors. This relation implies that we can discriminate optical-flow vectors on obstacle-region and the ground floor using the difference of the optical flow, if we have the optical-flow vectors on the ground floor as shown in Fig. 4(b). We call the relation of eq. (19) the spherical flow disparity.

5 Computation of the Navigation Direction using Visual Compass

Equation (16) implies the relation

$$\mathbf{v}(r, \phi + \pi, z) = \mathbf{v}(r, \phi, z), \quad (20)$$

since $\tan^2(\phi + \pi) = \tan^2 \phi$. Furthermore, equation (20) implies that the translation optical-flow vectors on the sphere satisfy the relation

$$|\mathbf{u}(\theta, \phi)| = |\mathbf{u}(\theta, \phi + \pi)| = |\mathbf{u}(\theta, -\phi)| = |\mathbf{u}(\theta, -\phi + \pi)|, \quad (21)$$

if there exist no obstacles on the ground floor. Therefore, the norm of the optical flow $|\mathbf{u}(\theta, \phi)|$ acts the potential to describe the obstacle area. Using the spherical disparity of optical flow, we define functions

$$d_F(\phi, a) = |\mathbf{u}(\theta_0 + a, \phi)| - |\mathbf{u}(\theta_0 + a, \pi - \phi)|, \quad (22)$$

$$d_B(\phi, a) = |\mathbf{u}(\theta_0 + a, \phi)| - |\mathbf{u}(\theta_0 + a, 2\pi - \phi)|, \quad (23)$$

for $\frac{\pi}{2} \leq \theta < \pi$ and $0 \leq \phi \leq \pi$, where the constant $\theta_0 > 0$ is the torrent measure to avoid colliding to the obstacle and $0 \leq a \leq \varepsilon \ll \rho_0$.

The function d_F detects the disparity of the lengths of optical flow vectors in the left and right of the front view. Furthermore, the function d_B detects the disparity of the lengths of optical flow vectors in the front view and back view. Therefore, these functions act as the gradients of the potential, from a side to the other side, and from the front to the back, respectively.

Form the potential and the gradients derived from the spherical optical flow fields, we have the following assertions for functions $d_F(\phi, a)$ and $d_B(\phi, a)$.

- If there is no obstacles on the ground floor, eq. (21) is satisfied and $d_F(\phi, a) = 0$.
- If $d_F(\phi, a) = 0$ and $d_B(\phi, a) = 0$, there exist no obstacles in front of the robot.
- If $d_F(\phi, 0) = 0$ and $d_B(\phi, a) \neq 0$, there exists the dead lock area in front of the robot.
- If $d_F(\theta, a) \neq 0$ and $\phi^* = \arg \max_{0 \leq \theta \leq \pi} d_F(\phi, 0)$, there exists an obstacle area in the direction $\mathbf{d} = (\cos \phi^*, \sin \phi^*, 0)^\top$.

From these assertions, we have the next control rules for the navigation direction.

If $d_F(\phi, a) = 0$, then move forward.

If $d_F(\phi, 0) = 0$ and $d_B(\phi, a) \neq 0$, turn to the backward.

If $d_F(\theta, a) \neq 0$ and $\phi^* = \arg \max_{0 \leq \theta \leq \pi} d_F(\phi, 0)$, then turn to the direction

$$\mathbf{d}^\perp = \begin{cases} (\cos(\phi^* + \frac{\pi}{2}), \sin(\phi^* + \frac{\pi}{2}), 0)^\top & \text{if } 0 < \phi^* < \frac{\pi}{2}, \\ (\cos(\phi^* - \frac{\pi}{2}), \sin(\phi^* - \frac{\pi}{2}), 0)^\top & \text{if } \frac{\pi}{2} < \phi^* < \pi. \end{cases}$$

The third rule turns the robot so that the obstacles lies in the side of the robot.

6 Numerical Results

In Fig. 6, the left, middle, and right show the results without obstacles, with obstacles, with a wall in front of the robot, respectively. From top to down, the spatial configuration, the panoramic optical flow, the norm of flow vectors on the equator of the spherical camera are shown, the gradient of the norm-based

potential, and the navigation direction are shown. These results show that our algorithm detects the disparities of the optical flow on the spherical retina.

Figure 6 shows a sequence of panoramic views in a real man-made environment and their optical flow fields. These views are panoramic views yielded from a sequence of images captured by a catadioptric imaging system mounted on a mobile robot. The optical flow fields are computed as the optical flow field on the spherical retina and transformed to the panoramic expression. The optical flow fields show the FOE and FOC. Furthermore, in the left-hand-side of the FOE, the optical flow vectors on the obstacles are detected. Furthermore, the lengths of flow vectors on the ground floor are short. This geometrical property means that it is possible to separate the free space for the navigation and obstacle regions from the flow field on the spherical retina, and it is possible to decide the navigation directions using the free space and obstacle region distribution on the spherical retina.

7 Conclusions

In this paper, we developed a visual navigation method for the robot mounting a spherical imaging system. The optical flow field on the spherical image yields monocular disparity as the difference of the optical flow vectors on the antipodal point on the equator assuming that the wheel-driven robot moves on a flat ground floor. This pair of antipodal vectors is used to compute the navigation direction.

Optical flow establishes the correspondences of points for the short-base stereo image pairs. This property derives the same geometric relations with binocular disparity. This monocular disparity on the spherical retina detects the geometrical configuration of the obstacles in the workspace. Therefore, this monocular disparity on the spherical retina enables the robot to navigate without any landmarks in the space.

In refs. [19, 17], optical-flow-based featureless and uncalibrated robot navigation strategies methods are proposed. In the former, a model-based method which uses the model optical flow field for the separation of obstacles on the ground floor is proposed. In the latter, as an extension of the first method, a featureless method is proposed. The later method used the optical flow of the one frame past pair images as the temporal model. Since the omnidirectional imaging systems capture both front and back views. This back view acts as the temporal model for the navigation for the panoramic-view-based visual navigation of the robot. Therefore, our spherical-image version requires no temporal images which are required in the method of ref.[17].

References

1. Baker, S. Nayer, S., A theory of single-viewpoint catadioptric image formation, *International Journal of Computer Vision*, **35**, 175-196, 1999.

2. Barreto, J., Daniilidis, K., Unifying image plane liftings for central catadioptric and dioptric cameras, *Proceedings of Omnivis04*, 151-162, 2004.
3. Brailon, C., C. Pradalier, C., Crowley, J.L., Laugier, C., Real-time moving obstacle detection using optical flow models, *Proceedings of Intelligent Vehicles Symposium*, 466-471, 2006.
4. Bur, A., Tapus, A., Ouerhani, N., Siegwar, R., Hiigli, H.: Robot navigation by panoramic vision and attention guided features, *Proceedings of ICPR06*, 695-698, 2006.
5. Daniilidis, K., Makadia, A., Bülow, T.: Image Processing in Catadioptric Planes: Spatiotemporal Derivatives and Optical Flow Computation, *Proceedings of OMNIVIS02*, 2002.
6. Franz, M. O., Mallot, H. A., Biomimetic robot navigation, *Robotics and Autonomous Systems*, **30**, 133-153, 2000.
7. Franz, M., Chahl, J., Krapp, H., Insect-inspired estimation of egomotion, *Neural Computation*, **16**, 2245-2260, 2004.
8. Gaspar, J., Winters, N., Santos-Victor, J., Vision-based navigation and environmental representations with an omnidirectional camera. *IEEE Trans. Robotics and Automation*, **16**, 890-898, 2000.
9. Geyer, C., Daniilidis, K., Catadioptric projective geometry, *International Journal of Computer Vision*, **45**, 223-243, 2001.
10. Green, W. E., Oh, P. Y., Barrows, G., Flying insect inspired vision for autonomous aerial robot maneuvers in near-earth environments, *Proceedings of ICRA04*, (2004)
11. Guilherme, N.D., Avinash, C.K., Vision for mobile robot navigation: A survey. *IEEE Trans. on PAMI*, **24**, 237-267, 2002.
12. Horn, B.K.P., Schunck, B.G., Determining optical flow. *Artificial Intelligence*, **17**, 185-203, 1981.
13. Karmeier, K., G. Krapp, H.G., Egelhaaf, M., Robustness of the tuning of fly visual interneurons to rotatory optic flow, *J Neurophysiol* **90**, 1626-1634, 2003.
14. Lopez-Franco, C., Bayro-Corrochano, E., Omnidirectional vision and invariant theory for robot navigation using conformal geometric algebra, *ICPR06*, 570-573, 2006.
15. Möller, R., Vardy, A., Local visual homing by matched-filter descent in image distances, *Biol Cybern*, **94**, 413-430, 2006.
16. Nayar, S., Catadioptric omnidirectional cameras, *Proceedings CVPR97*, 482-488, 1997.
17. Ohnishi, N., Imiya, A., Featureless robot navigation using optical flow, *Connection Science*, **17**, 23-46, 2005.
18. Sobey, P. J., Active navigation with a monocular robot, *Biol. Cybern.*, **71**, 433-440, 1994.
19. Santos-Victor, J. and Sandini, G., Uncalibrated obstacle detection using normal flow, *Machine Vision and Applications*, **9**, 130-137, 1996.
20. Tomic, I., Bogdanova, I., Frossard, P., Vandergheynst, P.: Multiresolution Motion Estimation for Omnidirectional Images, *Proceedings of EUSIPCO*, 2005
21. Vardy, A., Moller, R., Biologically plausible visual homing methods based on optical flow techniques, *Connection Science*, **17**, 47-89, 2005.
22. Winters, N., Gaspar, J., Lacey, J., Santos-Victor, J., Omni-directional vision for robot navigation, *Proceedings of Omnivis00*, 2000.
23. van der Zwaan, S., Santos-Victor, J., An Insect inspired visual sensor for the autonomous navigation of a mobile robot, *VisLab-TR 03/99*, 7th International Symposium on Intelligent Robotic Systems - SIRS99, Coimbra, Portugal, July 1999.

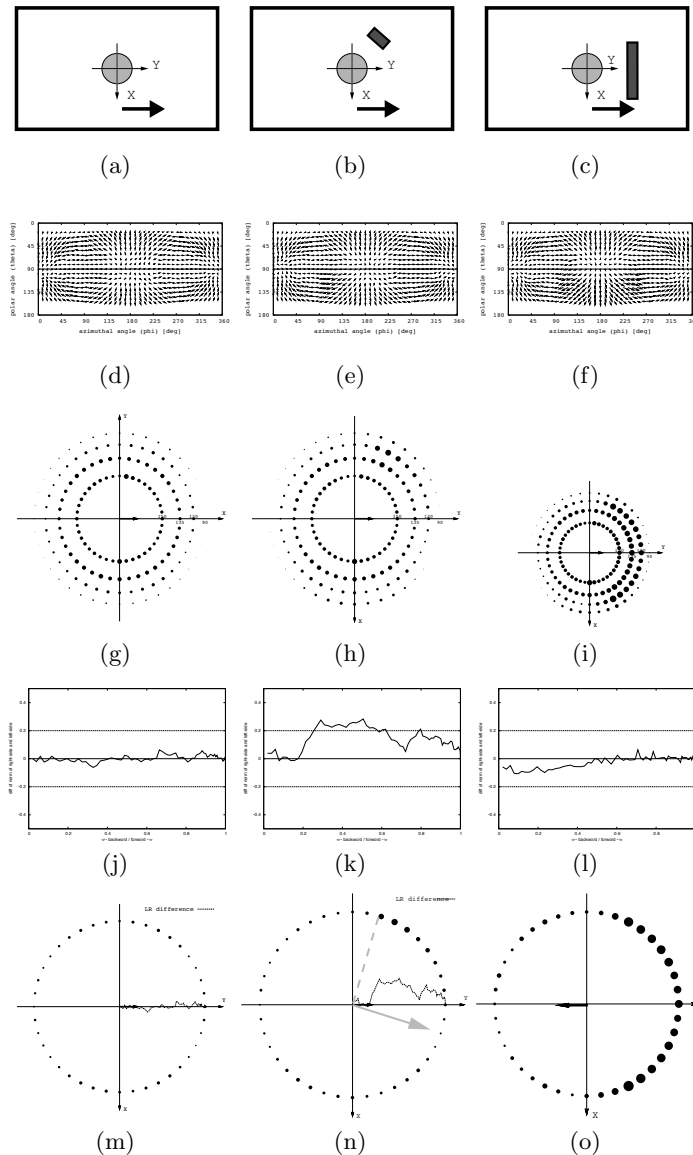
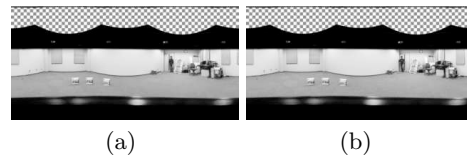
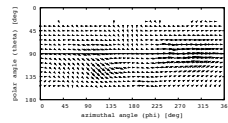


Fig. 4. Spherical optical flow. Left, middle, and right show the results without obstacles, with obstacles, and with a wall in front, respectively. From the top to the bottom: The configurations of the work spaces. The panoramic views of the optical flow fields computed on the spherical retina detect the obstacles as disparities of optical flow vectors. The length of the norm of flow vectors for $\theta = 90, 120, 135, 150$ degrees are plotted. The gradient of the potential induced by the norm of the optical flow vectors on $\theta = 120$ degree. The navigation direction computed using disparities of the optical flow vectors.

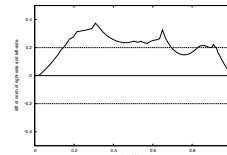


(a)

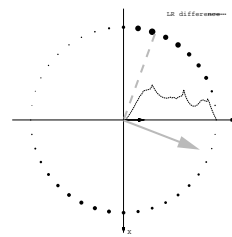
(b)



(c)



(d)



(e)

Fig. 5. Experiment for a real image sequence captured in a man-made environment. From the top to the bottom: The panoramic views of a pair of successive images from a sequence of panoramic views. The static obstacles (Boxes) and a dynamic obstacle (A man) exist in the views. The panoramic views of the optical flow fields computed on the spherical retina detect the obstacles as disparities of optical flow vectors. The gradient of the potential induced by the norm of the optical flow vectors on $\theta = 120$ degree. The navigation direction computed using disparities of the optical flow vectors.